ORIGINAL PAPER

Adsorption of sulfate from acid mine drainage in Northwestern China using Malan loess

Qiang Zheng[1] · Yongbo Zhang[1] · Yanrong Li[1] · Zhixiang Zhang[1] · Aijing Wu[1] · Hong Shi[1]

Abstract

Malan loess is a gray-yellow/brown-yellow, highly porous substance that has carbonate and calcium nodule late quaternary sediment formed by the accumulation of windblown dust. In this paper, the adsorption performances and mechanisms of sulfate adsorbed on Malan loess (Q3) were evaluated using batch adsorption experiments. The effects of the solid-to-liquid ratio, contact time, initial concentration, temperature, and pH on sulfate adsorption in acid mine drainage (AMD) were studied. The results indicated that sulfate adsorption capacity in loess increased with increasing contact time, initial concentration, and temperature, but decreased with an increased solid-to-liquid ratio. The acid condition was beneficial to the adsorption of sulfate. The optimal solid-to-liquid ratio was 100 g/L within the 50 to 800 g/L range, whilst the adsorption capacity and removal rate were 123.86 mg/g and 61.38%, respectively. XRD and FTIR analysis with or without sulfate adsorption demonstrated that calcite of loess played a key role during adsorption. Based on the results of batch experiments and physiochemical analysis, chemical adsorption was the dominant contributor. These results suggest that Malan loess is an applicable adsorbent for sulfate pollution.

Keywords Adsorption mechanisms · Isotherm · Kinetic · Malan loess · Sulfate removal

Introduction

Acid mine drainage (AMD) is a global environmental problem that is associated with mining activity (Kim and

✉ Yongbo Zhang
  zfstzhang@sina.com

  Qiang Zheng
  tyutzhengqiang@163.com

  Yanrong Li
  liyanrong@tyut.edu.cn

  Zhixiang Zhang
  zhangzhixiang@tyut.edu.cn

  Aijing Wu
  13546390360@sina.cn

  Hong Shi
  shihong@tyut.edu.cn

[1] College of Water Resources Science and Engineering, Taiyuan University of Technology, Taiyuan 030024, China

Yeongkyoo 2015; Moncur et al. 2014), which is generated from the oxidation of pyrite in the presence of bacteria (Blodau 2006; Chen et al. 2014; Pierre Louis et al. 2015). AMD is characterized by acidity and high concentrations of sulfate and heavy metal ions (Anawar 2015; MacIngova and Luptakova 2012; Modabberi et al. 2013; Ouyang et al. 2015). In recent years, AMD overflows have occurred due to the closure of many coal mines. This has led to AMD movement into superficial and subterranean waters, small streams, and rivers. AMD is therefore classed as a "long-term pollution source" (Ramla and Sheridan 2015; Galhardi and Bonotto 2016; Shim et al. 2015; Tischler et al. 2014; Gammons et al. 2010) and creates severe environmental problems in coal and gold mines. For example, AMD has been observed in various mining regions within Krugersdorp in South Africa, with sulfate concentrations of 3500 mg/L and pH ranging from 2 to 3 (Matsumoto et al. 2016). In China, the water quality of the Niangziguan spring in Shanxi province is severely affected by AMD from the abandoned mines in the Shandi River coal belt. In addition, the ecosystem was seriously damaged by AMD in acid mine areas, which caused the greenhouse effect. This accelerates climate change in the nearby environment as well as in forest, coastal, and urban areas (Cetin 2016a,

2016b.). Recently, mining using remote sensing and GIS has begun to solve problems related to water sources based on element characteristics (Kaya et al. 2018a, 2018b, Cetin et al. 2018).

The high concentrations of sulfate in AMD leads to pollution problems. Excessive sulfate negatively affects plant growth, disrupts the local ecological environment by acidifying soils and blocking soil pores which slows irrigation and water drainage (Bowell 2000), and causes diarrhea in humans (Backer and Lorraine 2000). AMD causes corrosion and scaling in pipes, structures, and equipment (Dehwah et al. 2002).

The maximum tolerable levels of sulfate in drinking water are 500 mg/L and 250 mg/L, as regulated by The World Health Organization (WHO) and China, respectively (WHO. 2011; GB 2006). As a consequence, efficient and cost-effective solutions to remove sulfate from AMD are urgently required. Sulfate removal methods include the following: (i) biological treatment by sulfate-reducing bacteria (SRB). Under anaerobic conditions, sulfate is reduced by SRB in the presence of organic substrates and the resulting sulfide can precipitate with metal ions to form stable metal sulfides which are stable and can be removed; (ii) chemical methods. Chemicals are used to decrease contaminants via converting them to inactive states; and (iii) adsorption methods using mineral materials. The remediation of sulfate with SRB is a promising alternative to conventional treatment methods. However, a limitation of SRB is that the low pH (pH < 4.0) of AMD inhibits the growth of microorganisms (Min et al. 2008; Sheoran et al. 2010; Hao et al. 2014; Sánchez-Andrea 2014; Bertolino et al. 2012). Although chemical treatment has been widely used as an alternative, it is expensive and leads to problems with chemical sludge treatment and disposal (Johnson and Hallberg 2005; Wu et al. 2002; Alemayehu and Lennartz 2010). Adsorption technologies are being increasingly considered as an attractive method due to their low cost and high efficiency.

In recent years, loess has been employed to adsorb contaminants (Zhu et al. 1983; Haque and Walmsley 1973; Jiang et al. 2010). Xie et al. (2017) investigated the adsorption properties of NH_4^+-N on Chinese loess and found that it effectively removed NH_4^+-N from aqueous solution. As reported by Tang et al. (2009), loess can also be used for Zn adsorption from aqueous solution and this process is influenced by the initial Zn concentration, pH, and temperature. Punrattanasin and Sariem (2015) determined that the adsorption of Cu, Zn, and Ni on red and yellow loess was influenced by contact time, the initial concentration of metal ions, and temperature. The adsorption capacity of yellow loess was higher than red loess. Cerqueira et al. (2011) assessed the adsorption of co-existing Cu and Cd in loess. The adsorption capacity of Cu was found to be higher than that of Cd. Compared to the soil, Chen and Liu 2014) found that organo-nano-clay had a relatively higher adsorption capacity for sulfate in aqueous solution. According to Zhao et al. (2017), sulfate adsorption in soil is mediated through electrostatic interactions and $CaSO_4$ formation, but biochar amendment does not increase the adsorption capacity of soil towards sulfate. Although loess has been proposed as an adsorbent of pollutants, studies on the various strata of loess are lacking.

In Northwestern China, loess is distributed in Shanxi, Shaanxi, Ningxia, Gansu, Inner Mongolia, and Henan. The loess-paleosol sequence in LPC typically consists of Wucheng loess (Q1), Lishi loess (Q2), and Malan loess (Q3) (Li et al. 2018). Malan loess is rich in carbonate and calcium nodules, possesses a large surface area, strong adsorption capabilities, high porosity, and excellent permeability. Furthermore, more than 60% of the coal mining area is overlaid with thick regions of loess. Thus, the abundance of loess provides the necessary materials for the treatment of AMD in the Shanxi province.

This study evaluated the adsorption performance and mechanism(s) of sulfate adsorbed onto Malan loess (Q3). Based on batch adsorption experiments, we assessed the effects of the solid-to-liquid ratio, contact time, initial concentration, temperature, and pH. In addition, the crystalline structure of the loess with or without adsorbed sulfate was determined by X-ray diffraction (XRD) and Fourier transform infrared spectroscopy (FTIR) to fully understand the mechanisms of loess adsorption.

Materials and Methods

Materials

Water samples were collected from the mine area of Yangquan City, Shanxi Province, China. They were stored in 10-L polyethylene bottle. The samples had a pH of 2.0 and a sulfate concentration of 20,180 mg/L, which was 80.72 times the maximum tolerable levels of sulfate in drinking water (GB 2006). The mine was in use for over 50 years prior to closing. Following closure, the AMD groundwater levels increased, and the water overflowed in certain locations, causing a potential risk to water resources and the environment.

The samples of Malan loess used in this study were obtained from a slope in Yangquan City, Shanxi Province, China, and were collected at a depth of 3.0 m to avoid plant roots. The samples were oven-dried at 105 °C for 24 h, cooled to room temperature, and passed through a 200-mesh-particle-size sieve. They were then stored in plastic bags until use. Clay (< 2 μm), silt (2–20 μm) and sand (> 20 μm) accounted for 1.56%, 22.64%, and 75.8%, respectively. The particle size was obtained using a particle size analyzer (Mastersizer 2000, China). Surface area was calculated using the Brunauer–Emmett–Teller (BET) method. The total pore volume including microspore volume was determined through

the levels of adsorbed N_2 under 0.99 pressure. The surface area, single point volume, and average pore diameter were 36.789 m² g⁻¹, 0.247 cm³ g⁻¹, and 26.896 nm, respectively. Compared with other soil, Malan loess had a larger specific surface area (Tang et al. 2009). The natural pH of loess was 8.05 which was measured using a radiometer PHM 250 ion analyzer.

Batch adsorption experiments

A series of batch adsorption experiments were performed to evaluate the adsorption performance and mechanisms of Malan loess. Adsorption kinetics were measured according to the solid-to-liquid, contact time, initial concentration, and temperature. Three replicates of all experiments were performed.

Experiments were performed at a range of solid-to-liquid ratios (50 g/L, 100 g/L, 200 g/L, 400 g/L, and 800 g/L) and adsorption times (5 min, 10 min, 0.5 h, 1 h, 2 h, 4 h, 8 h, 16 h, and 24 h) during shaking in a water bath at 270 rpm. Samples were separated from the suspension using a centrifugal separator at 5000 rpm for 5 min. Sulfate concentrations in the supernatants were analyzed through barium chromate spectrophotometry (λ = 440 nm, UV-vis spectrophotometry OVA, Lyz, Cyt) (GB/T 2006). To investigate the effects of the initial concentration, sulfate in AMD was diluted in deionized water at ratios of 1:0, 1:0.5, 1:1, 1:2, 1:4, 1:8, and 1:16. The pH of the solution was adjusted to 2.0 using 0.1 M HCl and NaOH. The effect of temperature was evaluated across the range of 15, 25, and 35 °C. To investigate the effect of solution pH on sulfate removal, appropriate amounts of either 0.1 M HCl or NaOH solutions were used to adjust the solution pH to 2.0–10.0.

The removal rate and adsorption capacity of sulfate adsorbed onto loess was calculated using Eqs.1 and 2. To investigate the rate law of sulfate onto loess, pseudo-first-order kinetics (Do 1998), pseudo-second-order kinetics (Do 1998) and the intra-particle diffusion model (Ho and Mckay 1998) were applied to fit the kinetic data. To investigate the sulfate adsorption of loess, Langmuir (Do 1998), Freundlich (Do 1998) and D–R isotherm models (Ho and Mckay 1998) were employed to fit the isotherm data.

The removal rate of sulfate (R) was calculated from the following equation:

$$R = \frac{C_0 - C_t}{C_0} \times 100 \tag{1}$$

The adsorption capacity of the loess was calculated using the following equation

$$q_t = \frac{(C_0 - C_t) \times V}{m} \tag{2}$$

where q_t (mg g⁻¹), at time, t, was the adsorption capacity, C_0 (mg L⁻¹) was the initial concentration of the solution, C_t (mg L⁻¹) was the residual concentration, V (L) was the volume of the solution, and m (g) was the mass of loess.

Loess characterization

The crystal structure of loess with or without adsorbing sulfate was determined using an X-ray diffractometer (XRD) with the radiation of copper Kα. The XRD pattern was scanned within the 2θ range from 0 to 65°, at a rate of 6.0° min⁻¹. Fourier transform infrared (FTIR) spectra (4000–500 cm⁻¹) were

Fig. 1 Effects of the solid-to-liquid ratio on the adsorption and removal of sulfate by loess (temperature = 25 °C ± 1 °C, pH = 2.0, initial sulfate C_0 = 20,180 mg/L, contact time = 24 h)
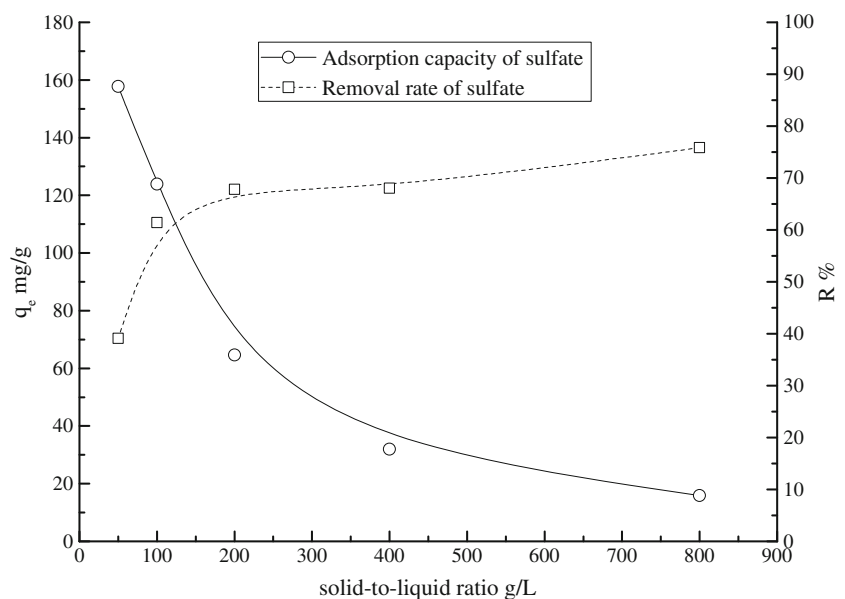
recorded using the TENSOR 27 model (BRUKER, Germany). The sample was thoroughly mixed with KBr (weight ratio of sample/KBr = 1%) in a mortar, and the fine powder was pressed into a pellet.

Results and discussion

Effect of the solid-to-liquid ratio

We first examined the effects of the solid-to-liquid ratio (50–800 g/L) on the adsorption of sulfate from AMD by loess (Fig. 1). The sulfate adsorption capacity sharply decreased at solid-to-liquid ratios of 50 to 200 g/L, and decreased more gradually from 200 to 800 g/L, likely due to the cementation and flocculation of loess. During assessment of the adsorption capacity, the sulfate removal ratio sharply increased from 50 to 100 g/L and then remained stable at higher solid-to-liquid ratios. Enhanced removal rates were primarily due to the increased number of available adsorption sites as the solid-to-liquid ratio increased. Here, the optimal solid-to liquid ratio was 100 g/L at which the sulfate adsorption capacity and removal rates were 123.86 mg/g and 61.38%, respectively. Similar observations had been reported (Liao and Shi 2005). At low solid-to-liquid ratios, potential adsorption sites on the loess were fully exposed and more quickly saturated, leading to higher adsorption values. However, at high solid-to-liquid ratios, potential binding sites were made unavailable due to particle aggregation, thus reducing the total surface area of the adsorbent and decreased the adsorption values.

Effects of contact time

The effect of contact time on sulfate adsorption onto loess is depicted in Fig. 2 at five solid-to-liquid ratios. The adsorption
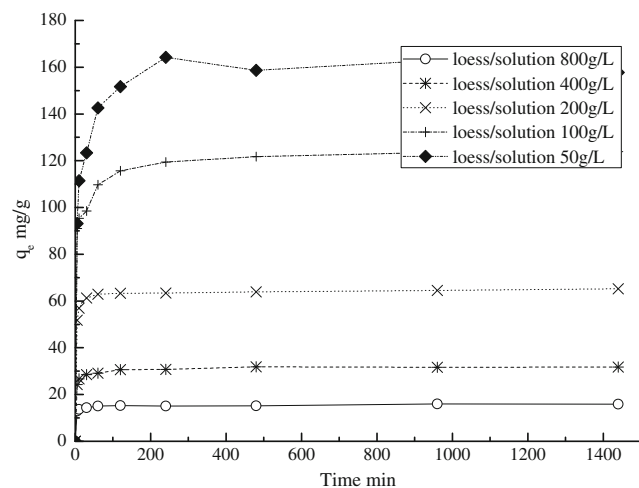

Fig. 2 Effects of contact time on sulfate adsorption by loess (temperature = 25 °C ± 1 °C, initial sulfate = C_0 20180mg/L, pH = 2.0)
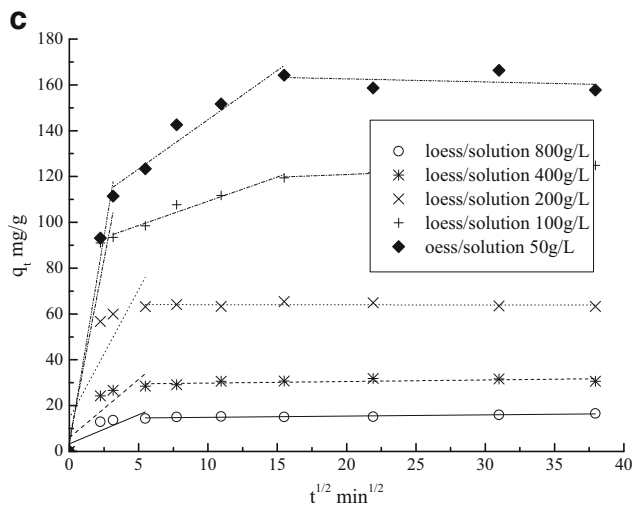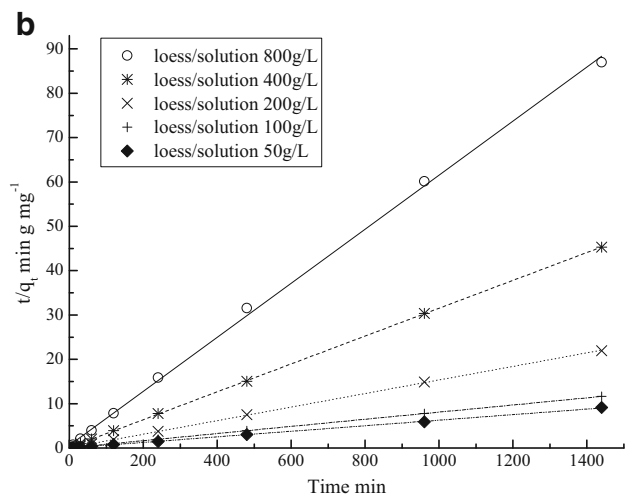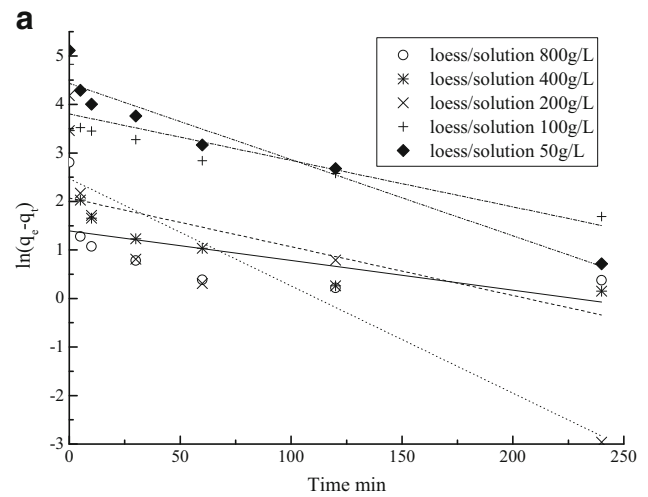
Fig 3 Fitted curves of the test data with **a** pseudo-first-order kinetics, **b** pseudo-second-order kinetics and **c** intra-particle diffusion model

of sulfate occurred rapidly in the first 30 min, reaching 80% of the maximum adsorption. Adsorption then slowed till reaching an equilibrium at 960 and 480 min in the range of

Table 1   Parameters of the kinetic models

Model	Parameter	Solid-to-liquid ratio (g/L)				
		800	400	200	100	50
Pseudo-first-order kinetics	q_e (mg g^{-1})	4.035	7.516	11.834	44.88	84.352
	$k_1 (\times 10^{-3}$ min^{-1})	6.112	10.05	22.11	9.58	15.72
	R^2	0.3583	0.5968	0.7911	0.7474	0.9412
Pseudo-second-order kinetics	q_e (mg g^{-1})	16.39	31.85	65.36	123.46	158.73
	$k_2 (\times 10^{-3}$ g mg^{-1} min^{-1})	6.54	9.46	4.17	1.417	2.54
	$k_2.q_e^2$ (mg g^{-1} min^{-1})	1.76	9.60	17.81	21.60	63.99
	R^2	0.9991	1	0.9999	1	0.9996
Intra-particle diffusion model	k_{int1} (mg g^{-1} min$^{-1/2}$)	2.553	5.098	11.25	31.6	36.41
	C_1	3.296	5.998	14.39	4.615	2.653
	R_1^2	0.7148	0.7501	0.7185	0.9306	0.9818
	k_{int2} (mg g^{-1} min$^{-1/2}$)				2.114	4.296
	C_2				88.04	101.94
	R_2^2				0.9628	0.9446

50 to 100 g/L and 200 to 800 g/L, respectively. The calcite of loess dissolved in strong acidic solution, then combined with the sulfate and was adsorbed onto the loess surface, which limited the adsorption. To make sure of sufficient contact time, other batch experiments (solid-to liquid ratio was 100 g/L) were carried out for 24.0 h.

To further explore the sulfate adsorption process, kinetic data were fitted using pseudo-first-order, pseudo-second-order, and intra-particle diffusion models. The results are presented in Fig. 3 and the corresponding parameters are listed in Table 1. According to the highest correlation coefficient $R^2 >$ 0.999 (Table 1), the theoretical $q_{e,cal}$ values were consistent with the experimental q_e values (q_e = 15.93 mg g^{-1}, 31.90 mg g^{-1}, 65.50 mg g^{-1}, 123.08 mg g^{-1}, 160.92 mg g^{-1} at solid-to-

liquid ratios of 800 g/L, 400 g/L, 200 g/L, 100 g/L and 50 g/L). Thus, the adsorption kinetics of sulfate onto loess were most accurately described by the pseudo-second-order model. The results indicated that the adsorption process was dominated by the chemical reaction (Koumaiti et al. 2011). Figure 3c demonstrated that the linear fit of the diffusion model of sulfate adsorption particles was a multi-stage process (Zhao et al. 2017). The three stages of the adsorption process which occurred at solid-to-liquid ratios of 50 g/L and 100 g/L were rapid external surface adsorption, gradual internal diffusion, and final equilibration. However, at higher solid-to-liquid ratios including 200 g/L, 400 g/L and 800 g/L, no second linear portion was observed during the adsorption process. The plots did not pass through the origin, suggesting that the adsorption was complex and involves both surface adsorption and intra-particle diffusion.

Effects of initial concentration and temperature

The influence of the initial concentration and temperature on sulfate adsorption by loess is shown in Fig. 4.

The increase in adsorption capacity was low at sulfate equilibrium concentrations of 0 to 1000 mg/L, and rapidly increased from 1000 to 6000 mg/L. The concentration gradient of sulfate on the interface between loess and the solution
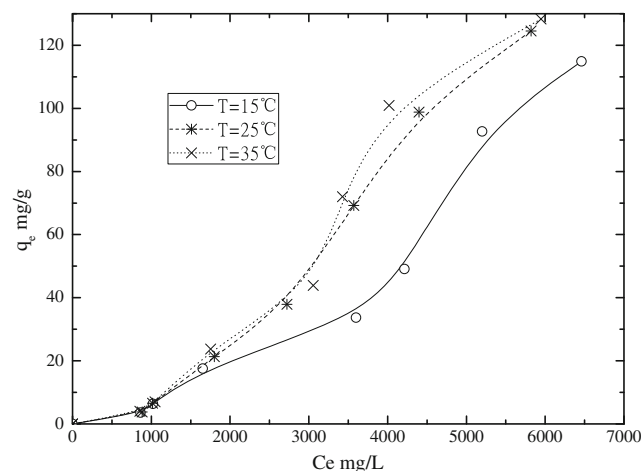

Fig 4 Effects of the initial concentration on the adsorption of sulfate by loess at different temperatures (initial sulfate concentration: solution-deionized water ratios 1:0, 1:0.5, 1:1, 1:2, 1:4, 1:8, and 1:16, contact time = 24 h, solid-to-liquid ratio = 100 g/L, pH = 2.0)

Table 2   Thermodynamic parameters for sulfate adsorption onto loess

T(K)	ΔG^0 (kJ mol^{-1})	ΔH^0 (kJ mol^{-1})	ΔS^0 (J mol^{-1} K^{-1})
288.15	-1.27	11.05	43.10
298.15	-2.02		
308.15	-2.12		

increased as initial concentrations increased, as elevated sulfate concentrations provided the necessary driving force to overcome mass transfer resistance between the liquid and solid phases. Compared with the sulfate concentration, although
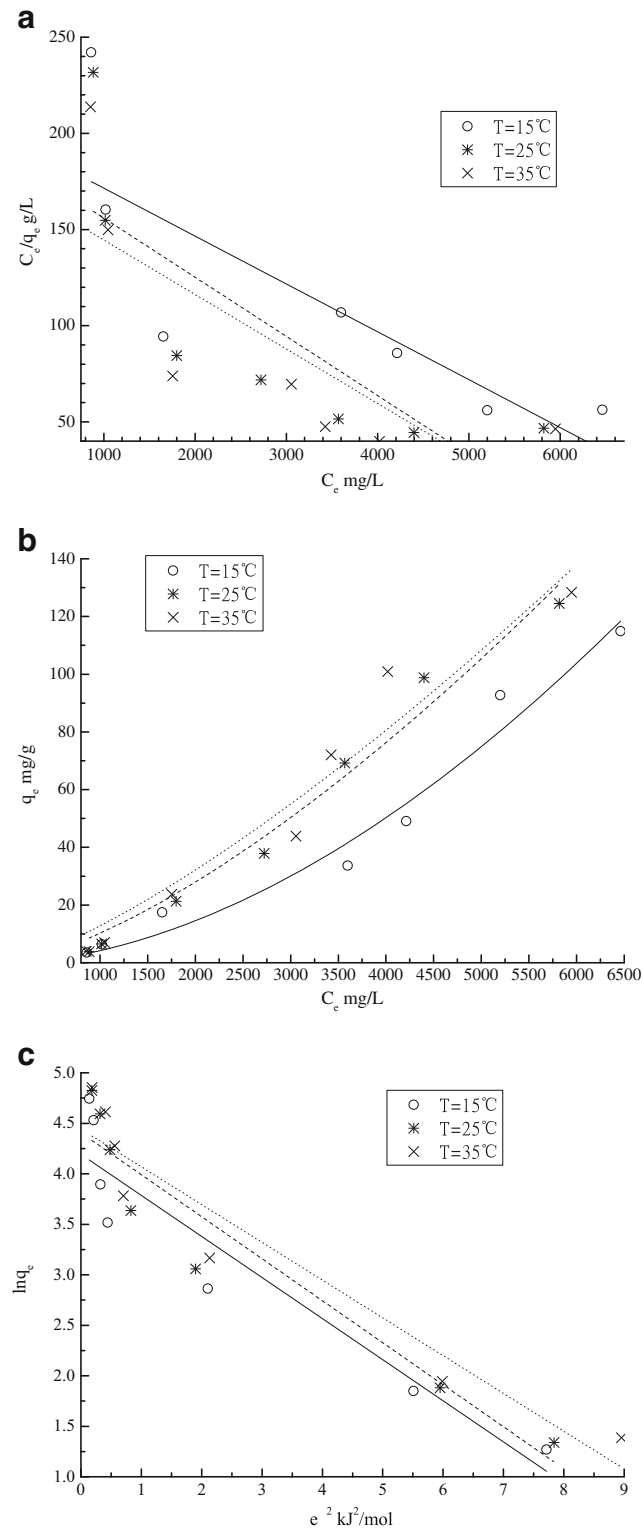
Fig. 5 Adsorption isotherms. **a** Langmuir model. **b** Freundlich model. **c** D–R model

Table 3 Parameters of the isotherm models

Model	Parameter	Temperature(°C)		
		15 °C	25 °C	35 °C
Langmuir	q_{m} (mg g^{-1})	45.95	32.49	35.29
	B (L mg^{-1})	0.000125	0.000165	0.000164
	R^2	0.5906	0.6421	0.6135
Freundlich	K (mg g^{-1})	0.2692	4.699	13.53
	n	1.743	1.447	1.326
	R^2	0.9648	0.9797	0.9456
D–R	q_{m} (mg g^{-1})	68.375	82.023	85.115
	k	0.4078	0.4159	0.374
	R^2	0.9077	0.919	0.9181

the adsorption capacity of sulfate improved with the temperature increasing, the latter only had a smaller effect on its adsorption capacity.

In order to investigate nature of the adsorption process, thermodynamic parameters (ΔG^0, ΔH^0, ΔS^0) were estimated according to Eqs. 3–5. (Sadik et al. 2015).

$$k = \frac{q_e}{c_e} \tag{3}$$

$$\Delta G^0 = -RT \ln k \tag{4}$$

$$\ln k = \frac{\Delta S^0}{R} - \frac{\Delta H^0}{RT} \tag{5}$$

where R is the universal gas constant (8.314 J mol^{-1} K^{-1}); k is an adsorption equilibrium constant; the linear curve was fitted using $1/T$ versus $\ln k$. The changes in standard enthalpy (ΔH^0) and standard entropy (ΔS^0) were calculated based on the slope and intercept, respectively.
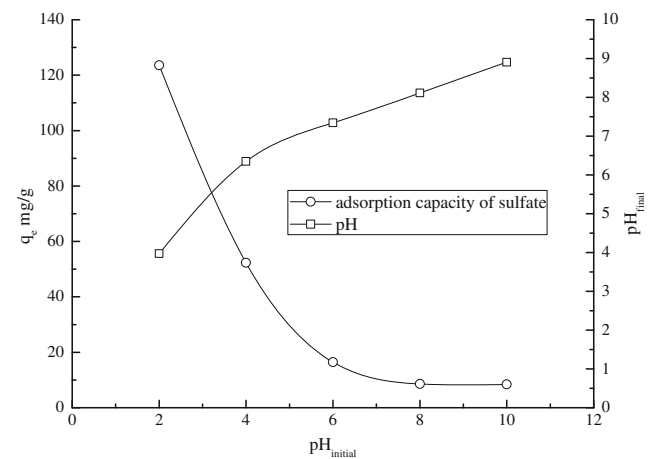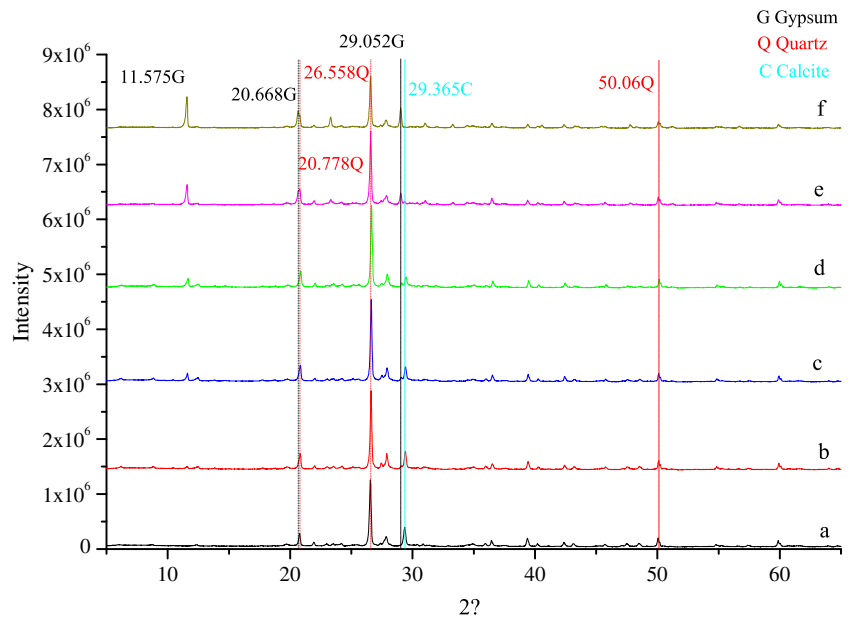

Fig. 6 Effects of solution pH on the adsorption of sulfate by loess (temperature = 25 °C ± 1 °C, initial sulfate = C_0 20180mg/L, contact time = 24 h, solid-to-liquid ratio = 100 g/L)

Fig. 7 XRD patterns of the loess before and after sulfate adsorption at different solid-to-liquid ratios. **a** Loess. **b–f** Solid-to-liquid ratio 800 g/L, 400 g/L, 200 g/L, 100 g/L, 50 g/L

The calculated thermodynamic parameters are listed in Table 2. The negative values of ΔG^0 and positive ΔH^0 implied that the adsorption of sulfate on loess was spontaneous and endothermic in nature. The positive value of ΔS^0 indicated that randomness, or entropy, increased at the solid-liquid interface during adsorption process. Similar results were observed in previous studies (Chen et al. 2014). It was possible that the increased temperature promoted the sulfate-loess interaction, increased sulfate mobility, and reduced the mass transfer resistance to diffusion ions. In future experiments, the adsorption of loess under freezing/thawing environmental conditions should be considered.

The isotherm data were further analyzed using the Langmuir isotherm, Freundlich isotherm, and D–R isotherm adsorption models to highlight the interaction between loess and sulfate. The results are presented in Fig. 5 and the corresponding parameters are listed in Table 3. Compared with the other two models, the Freundlich isotherm model gave a higher correlation coefficient (R^2), indicating that the adsorption of sulfate onto loess did not occur on a monolayer, but on a heterogeneous surface with different adsorption sites (Do 1998). Moreover, according to Table 3, n was larger than unity, which increased with increasing temperature, indicating that the adsorption was favorable (Vasiliu et al. 2011).
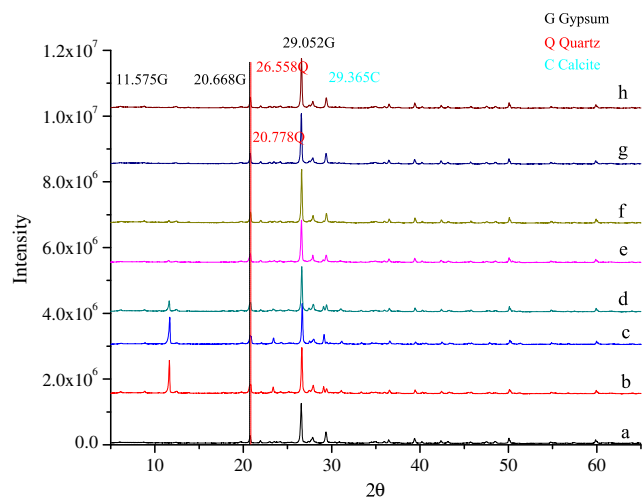

Fig. 8 XRD patterns of loess before and after sulfate adsorption at a range of initial concentrations. **a** Loess. **b–h** Solution-deionized water ratios 1:0, 1:0.5, 1:1, 1:2, 1:4, 1:8, and 1:16
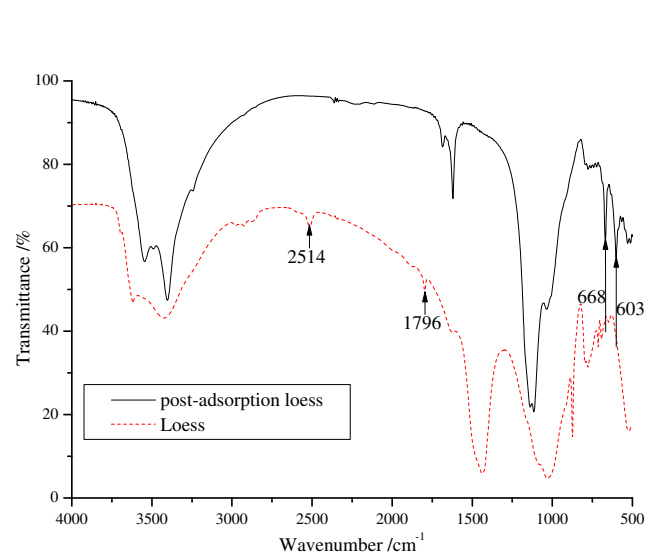

Fig. 9 FTIR spectra of loess before and after sulfate adsorption

Effects of pH on sulfate adsorptions

The effects of pH, ranging from 2.0 to 10.0, on the sulfate adsorbed onto the loess are shown in Fig. 6. Sulfate adsorption by loess was strongly dependent on pH and adsorption capacity sharply decreased as pH increased from 2.0 to 6.0, then decreased gradually from 6.0 to 10.0. Similar trends had been previously observed in other adsorbents (Sadik et al. 2015; Zhao et al. 2017). The surface of loess was positively charged by protonation with H^+, which led to increased anionic adsorption through electrostatic attraction. Meanwhile, the calcite component of loess dissolved in strong acidic solution and combined with sulfate. However, the loess surface was negatively charged in alkaline solutions, which repelled the negative anionic (SO_4^{2-}). Moreover, it was possible that OH^- could compete with SO_4^{2-} for loess adsorption sites, and that this could decrease the amount of sulfate adsorbed. Figure 6 showed that the pH_{final} increased when $pH_{initial} < 8.0$, indicating that loess has a buffering effect on acidic solution. At $pH_{initial} > 8.0$, the pH_{final} shifted to lower values than $pH_{initial}$.

Adsorption mechanism

To clarify the sulfate adsorption mechanism(s), the crystalline structure of loess with or without sulfate was determined by XRD. The results are shown in Figs. 7 and 8 with corresponding solid-to-liquid ratios and initial concentrations, respectively. Figures 7a and 8a were natural Malan loess, mainly composed of quartz, calcite, clay, and albite. When sulfate was adsorbed onto this loess, the diffraction peak of calcite ($CaCO_3$) at $2\theta = 29.365°$ decreased, and three diffraction peaks of gypsum ($CaSO_4 \cdot 2H_2O$) at $2\theta = 11.575°$, $20.668°$, and $29.052°$ appeared. This demonstrated that calcite played a key role in sulfate adsorption onto loess through chemical adsorption that was dependent on $CaSO_4$. The intensity of gypsum gradually increased with decreasing solid-to-liquid ratios, and also increased with increasing soil-water ratios, which indicated an increased adsorption capacity (Figs. 7 and 8) (Chung and IUCr 1975; Mehmet 2013). This result was consistent with Figs. 1 and 4.

Figure 9 shows the FTIR spectra of the loess with or without adsorbing sulfate. For natural loess, the intense bands at 1796 cm^{-1} and 2514 cm^{-1} were assigned to C=O (Xie et al. 2017; Wang et al. 2009). After sulfate was adsorbed onto the loess, new characteristic peaks were observed as a doublet at 668 cm^{-1} and 603 cm^{-1} due to the bending vibration of the sulfate (Anbalagan et al. 2009), and the peaks at 1796 cm^{-1} and 2514 cm^{-1} disappeared. This implied that the loess calcite dissolved in AMD, combined with the sulfate, and was adsorbed onto the loess surface. The combined results of XRD and FTIR confirmed that calcite played a key role in the chemical adsorption of sulfate from AMD.

Conclusions

This study investigated the adsorption of sulfate onto Malan loess through batch adsorption experiments. The capacity of loess to adsorb sulfate from AMD was dependent on the solid-to-liquid ratio, contact time, and initial concentration. The sulfate adsorption capacity increased with increasing adsorption time and initial concentration, but decreased with increasing solid-to-liquid ratio. Although thermodynamic analysis showed that the adsorption was spontaneous and endothermic, the adsorption capacity was modestly influenced by temperature ranging from 15 to 35 °C. Acidic conditions were beneficial to the adsorption of sulfate. The optimal solid-to-liquid ratio for sulfate adsorbed onto loess was 100 g/L ranging from 50 to 800 g/L, while the adsorption capacity and removal rates were 123.86 mg/g and 61.38%, respectively. The adsorption of sulfate onto loess was well described by the pseudo-second-order function. The Freundlich isotherm model gave the best fit for the equilibrium data for sulfate adsorption onto loess as compared to the other two isotherm models, indicating a heterogeneous adsorbent surface. XRD and FTIR analysis demonstrated that the loess calcite played a key role during adsorption. Based on the results of batch experiments and physiochemical analysis, chemical adsorption was the dominant adsorption mechanism. In conclusion, the low cost of loess and its ease of availability make it a potentially attractive sulfate adsorbent in AMD. Loess loaded with sulfate can be safely disposed of in landfills and burned after drying. Further experiments will be required to assess the adsorption of sulfate onto loess in a freezing/thawing environment.

Compliance with ethical standards

Conflict of interest The authors declare that they have no conflict of interest.

References

Kaya E, Agca M, Adiguzel F, Cetin M (2018a) Spatial data analysis with r programming for environment. Hum Ecol Risk Assess (1):1–10. https://doi.org/10.1080/10807039.2018.1470896

Alemayehu E, Lennartz B (2010) Adsorptive removal of nickel from water using volcanic rocks. Appl Geochem 25:1596–1602. https://doi.org/10.1016/j.apgeochem.2010.08.009

Anawar HM (2015) Sustainable rehabilitation of mining waste and acid mine drainage using geochemistry, mine type, mineralogy, texture, ore extraction and climate knowledge. J Environ Manag 158:111–121. https://doi.org/10.1016/j.jenvman.2015.04.045

Anbalagan G, Mukundakumari S, Murugesan KS, Gunasekaran S (2009) Infrared, optical absorption, and epr spectroscopic studies on natural gypsum. Vib Spectrosc 50:226–230. https://doi.org/10.1016/j.vibspec.2008.12.004

Backer, Lorraine C (2000) Assessing the acute gastrointestinal effects of ingesting naturally occurring, high levels of sulfate in drinking water. Crit Rev Clin Lab Sci 37:389–400. https://doi.org/10.1080/10408360091174259

Bertolino SM, Rodrigues ICB, Guerra-Sá R, Aquino SF, Leão VA (2012) Implications of volatile fatty acid profile on the metabolic pathway during continuous sulfate reduction. J Environ Manag 103:15–23. https://doi.org/10.1016/j.jenvman.2012.02.022

Blodau C (2006) A review of acidity generation and consumption in acidic coal mine lakes and their watersheds. Sci Total Environ 369:307–332. https://doi.org/10.1016/j.scitotenv.2006.05.004

Bowell RJ (2000). Sulphate and salt minerals: the problem of treating mine waste. Mining Environmental Management 5:11–14

Cerqueira B, Covelo EF, Andrade L, Vega FA (2011) The influence of soil properties on the individual and competitive sorption and desorption of Cu and Cd. Geoderma 162:20–26. https://doi.org/10.1016/j.geoderma.2010.08.013

Cetin M, Adiguzel F, Kaya O, Sahap A (2018) Mapping of bioclimatic comfort for potential planning using GIS in Aydin. Environ Dev Sustain 20(1):361–375. https://doi.org/10.1007/s10668-016-9885-5

Cetin M (2016a) Determination of bioclimatic comfort areas in landscape planning: a case study of Cide Coastline. Turkish Journal of Agriculture-Food Science and Technology 4(9):800–804. https://doi.org/10.24925/turjaf.v4i9.800-804.872

Cetin M (2016b) Sustainability of urban coastal area management: a case study on Cide. J Sustain For 35(7):527–541. https://doi.org/10.1080/10549811.2016.1228072

Chen YT, Li JT, Chen LX, Hua ZS, Huang LN, Liu J, Xu BB, Liao B, Shu WS (2014) Biogeochemical processes governing natural pyrite oxidation and release of acid metalliferous drainage. Environ Sci Technol 48:5537–5545. https://doi.org/10.1021/es500154z

Chen W, Liu HC (2014) Adsorption of sulfate in aqueous solutions by organo-nano-clay: adsorption equilibrium and kinetic studies. J Cent South Univ 21:1974–1981. https://doi.org/10.1007/s11771-014-2145-7

Chung FH, IUCr (1975) Quantitative interpretation of x-ray diffraction patterns of mixtures. iii. Simultaneous determination of a set of reference intensities. J Appl Crystallogr 8:17–19. https://doi.org/10.1107/S0021889875009454

Dehwah HAF, Maslehuddin M, Austin SA (2002) Long-term effect of sulfate ions and associated cation type on chloride-induced reinforcement corrosion in Portland cement concretes. Cem Concr Compos 24:17–25. https://doi.org/10.1016/S0958-9465(01)00023-3

Do DD (1998) Adsorption analysis: equilibrium and kinetics. Imperial College Press, London, pp 13–50

Galhardi JA, Bonotto DM (2016) Hydrogeochemical features of surface water and groundwater contaminated with acid mine drainage (AMD) in coal mining areas: a case study in southern Brazil. Environ Sci Pollut Res 23:18911–18927. https://doi.org/10.1007/s11356-016-7077-3

Gammons CH, Duaime TE, Parker SR, Poulson SR, Kennelly P (2010) Geochemistry and stable isotope investigation of acid mine drainage associated with abandoned coal mines in central Montana, USA. Chem Geol 269:100–112

GB 5749 (2006) Ministry of health in China. Standards for drinking water quality [S]. (In Chinese)

GB/T 5750.5 (2006) Standard examination methods for drinking water—nonmetal parameters [S]. (In Chinese)

Haque I, Walmsley D (1973) Adsorption and desorption of sulphate in some soils of the West Indies. Geoderma 9:269–278. https://doi.org/10.1016/0016-7061(73)90028-1

Hao T, Xiang P, Mackey HR, Chi K, Lu H, Chui H, van Loosdrecht MCM, Chen GH (2014) A review of biological sulfate conversions in wastewater treatment. Water Res 65:1–21. https://doi.org/10.1016/j.watres.2014.06.043

Ho YS, Mckay G (1998) A comparison of chemisorption kinetic models applied to pollutant removal on various sorbents. Process Saf Environ Prot 76:332–340. https://doi.org/10.1205/095758298529696

Jiang MQ, Jin XY, Lu XQ, Chen Zl (2010) Adsorption of Pb (II), Cd (II), Ni (II) and Cu (II) onto natural kaolinite clay. Desalination 252:33–39. https://doi.org/10.1016/j.desal.2009.11.005

Johnson DB, Hallberg KB (2005) Acid mine drainage remediation options: a review. Sci Total Environ 338:3–14. https://doi.org/10.1016/j.scitotenv.2004.09.002

Kaya E, Agca M, Adiguzel F, Cetin M (2018b) Spatial data analysis with r programming for environment. Hum Ecol Risk Assess:1), 1–1),10. https://doi.org/10.1080/10807039.2018.1470896

Kim, Yeongkyoo (2015) Mineral phases and mobility of trace metals in white aluminum precipitates found in acid mine drainage. Chemosphere 119:803–811. https://doi.org/10.1016/j.chemosphere.2014.08.034

Koumaiti S, Riahi K, Ounaies F, Ben TB (2011) Kinetic modelling of liquid-phase adsorption of sulfate onto raw date palm seeds. J Environ Sci Eng 5:1570–1580

Li Y, He S, Deng X, Xu Y (2018) Characterization of macropore structure of Malan loess in NW China based on 3D pipe models constructed by using computed tomography technology. J Asian Earth Sci 154:271–279. https://doi.org/10.1016/j.jseaes.2017.12.028

Liao XP, Shi B (2005) Adsorption of fluoride on zirconium (IV)-impregnated collagen fiber. Environ Sci Technol 39:4628–4632. https://doi.org/10.1021/es0479944

MacIngova E, Luptakova A (2012) Recovery of metals from acid mine drainage. Chem Eng Trans 28:109–114. https://doi.org/10.3303/CET1228019.

Matsumoto S, Shimada H, Sasaoka T (2016) The key factor of acid mine drainage (AMD) in the history of the contribution of mining industry to the prosperity of the United States and South Africa: a review. Nat Resour 7:445–460. https://doi.org/10.4236/nr.2016.77039

Mehmet T (2013) Quantitative phase analysis based on rietveld structure refinement for carbonate rocks. J Mod Phys 4:1149–1157. https://doi.org/10.4236/jmp.2013.48154

Min X, Chai L, Zhang C, Takasaki Y, Okura T (2008) Control of metal toxicity, effluent COD and regeneration of gel beads by immobilized sulfate-reducing bacteria. Chemosphere 72:1086–1091. https://doi.org/10.1016/j.chemosphere.2008.04.001

Modabberi S, Alizadegan A, Mirnejad H, Esmaeilzadeh E (2013) Prediction of AMD generation potential in mining waste piles, in the Sarcheshmeh porphyry copper deposit, Iran. Environ Monit Assess 185:9077–9087. https://doi.org/10.1007/s10661-013-3237-9

Moncur MC, Ptacek CJ, Hayashi M, Blowes DW, Birks SJ (2014) Seasonal cycling and mass-loading of dissolved metals and sulfate discharging from an abandoned mine site in northern Canada. Appl

Geochem 41:176–188. https://doi.org/10.1016/j.apgeochem.2013.12.007

Ouyang Y, Liu Y, Zhu RL, Ge F, Xu TY, Luo Z, Liang LB (2015) Pyrite oxidation inhibition by organosilane coatings for acid mine drainage control. Miner Eng 72:57–64. https://doi.org/10.1016/j.mineng.2014.12.020

Pierre Louis AM, Yu H, Shumlas SL, Van Aken B, Schoonen MAA, Strongin DR (2015) Effect of phospholipid on pyrite oxidation and microbial communities under simulated acid mine drainage (AMD) conditions. Environ Sci Technol 49:7701–7708. https://doi.org/10.1021/es505374g

Punrattanasin P, Sariem P (2015) Adsorption of copper, zinc, and nickel using loess as adsorbents. Pol J Environ Stud 24:1259–1266. https://doi.org/10.15244/pjoes/30264

Ramla B, Sheridan C (2015) The potential utilisation of indigenous South African grasses for acid mine drainage remediation. Water SA 41:247–251. https://doi.org/10.4314/wsa.v41i2.10

Sadik R, Lahkale R, Hssaine N, ElHatimi W, Diouri M, Sabbar E (2015) Sulfate removal from wastewater by mixed oxide-LDH: equilibrium, kinetic and thermodynamic studies. J Mater Environ Sci 6:2895–2905

Sánchez-Andrea I (2014) Sulfate reduction at low pH to remediate acid mine drainage. J Hazard Mater 269:98–109. https://doi.org/10.1016/j.jhazmat.2013.12.032

Sheoran AS, Sheoran V, Choudhary RP (2010) Bioremediation of acid-rock drainage by sulphate-reducing prokaryotes: a review. Miner Eng 23:1073–1100. https://doi.org/10.1016/j.mineng.2010.07.001

Shim MJ, Choi BY, Lee G, Hwang YH, Yang JS, O'Loughlin EJ et al (2015) Water quality changes in acid mine drainage streams in Gangneung, Korea, 10 years after treatment with limestone. J Geochem Explor 159:234–242. https://doi.org/10.1016/j.gexplo.2015.09.015

Tang X, Li Z, Chen Y, Wang Z (2009) Removal of Zn (II) from aqueous solution with natural Chinese loess: behaviors and affecting factors. Desalination 249:49–57. https://doi.org/10.1016/j.desal.2008.10.023

Tischler JS, Wiacek C, Janneck E, Schlömann M (2014) Bench-scale study of the effect of phosphate on an aerobic iron oxidation plant for mine water treatment. Water Res 48:345–353. https://doi.org/10.1016/j.watres.2013.09.049

Vasiliu S, Bunia I, Racovita S, Neagu V (2011) Adsorption of cefotaxime sodium salt on polymer coated ion exchange resin microparticles: kinetics, equilibrium and thermodynamic studies. Carbohydr Polym 85:376–387. https://doi.org/10.1016/j.carbpol.2011.02.039

Wang Y, Tang X, Chen Y, Zhan L, Li Z, Tang Q (2009) Adsorption behavior and mechanism of Cd (II) on loess soil from china. J Hazard Mater 172:30–37. https://doi.org/10.1016/j.jhazmat.2009.06.121

WHO (ed) (2011) Guidelines for drinking-water quality, Fourth edn. WHO Press, Geneva

WU CH, Kuo CY, Lin CF et al (2002) Modeling competitive adsorption of molybdate, sulfate, selenate, and selenite using a Freundlich-type multi-component isotherm. Chemosphere 47:283–292. https://doi.org/10.1016/S0045-6535(01)00217-X

Xie H, Wang S, Qiu Z, Jiang J (2017) Adsorption of NH4 + -N on Chinese loess: non-equilibrium and equilibrium investigations. J Environ Manag 202:46–54. https://doi.org/10.1016/j.jenvman.2017.07.016

Zhao B, Nan X, Xu H, Zhang T, Ma F (2017) Sulfate sorption on rape (Brassica campestris L.) straw biochar, loess soil and a biochar-soil mixture. J Environ Manag 201:309–314. https://doi.org/10.1016/j.jenvman.2017.06.064

Zhu XM, Li YS, Peng XL, Zhang SG (1983) Soils of the loess region in China. Geoderma 29:237–255. https://doi.org/10.1016/0016-7061(83)90090-3